

Iron nitrides: High-pressure synthesis, nitrogen disordering and local magnetic moment

Yu Tao(陶雨) and Li Lei(雷力)

Citation: Chin. Phys. B, 2025, 34 (**6**): 068301. DOI: 10.1088/1674-1056/adca1c
Journal homepage: http://cpb.iphy.ac.cn; http://iopscience.iop.org/cpb

What follows is a list of articles you may be interested in

Optimization of Skanavi model and its application to high permittivity materials

Hao Luo(罗昊), Xinrui Qin(秦新瑞), Kejia Geng(耿可佳), Cuncun Kong(孔存存), and Pengfei Cheng(成鹏飞)
Chin. Phys. B, 2025, 34 (**1**): 017702. DOI: 10.1088/1674-1056/ad9ba0

Facile integration of an Al-rich $Al_{1-x}In_xN$ photodetector on free-standing GaN by radio-frequency magnetron sputtering

Xinke Liu(刘新科), Zhichen Lin(林之晨), Yuheng Lin(林钰恒), Jianjin Chen(陈建金), Ping Zou(邹苹), Jie Zhou(周杰), Bo Li(李博), Longhai Shen(沈龙海), Deliang Zhu(朱德亮), Qiang Liu(刘强), Wenjie Yu(俞文杰), Xiaohua Li(黎晓华), Hong Gu(顾泓), Xinzhong Wang(王新中), and Shuangwu Huang(黄双武)
Chin. Phys. B, 2023, 32 (**11**): 117701. DOI: 10.1088/1674-1056/acbf25

SiC gate-controlled bipolar field effect composite transistor with polysilicon region for improving on-state current

Baoxing Duan(段宝兴), Kaishun Luo(罗开顺), and Yintang Yang(杨银堂)
Chin. Phys. B, 2023, 32 (**4**): 047702. DOI: 10.1088/1674-1056/ac80ab

Hybrid-anode structure designed for a high-performance quasi-vertical GaN Schottky barrier diode

Qiliang Wang(王启亮), Tingting Wang(王婷婷), Taofei Pu(蒲涛飞), Shaoheng Cheng(成绍恒),Xiaobo Li(李小波), Liuan Li(李柳暗), and Jinping Ao(敖金平)
Chin. Phys. B, 2022, 31 (**5**): 057702. DOI: 10.1088/1674-1056/ac272a

Steady and transient behavior of perylene under high pressure

Ting-Ting Wang(王亭亭), Yu Zhang(张宇), Hong-Yu Tu(屠宏宇), Lu Han(韩露), Ji-Chao Cheng(程基超), Xin Wang(王鑫), Fang-Fei Li(李芳菲), Ling-Yun Pan(潘凌云), and Tian Cui(崔田)
Chin. Phys. B, 2021, 30 (**11**): 118201. DOI: 10.1088/1674-1056/abf923

TOPICAL REVIEW — Structures and properties of materials under high pressure

Iron nitrides: High-pressure synthesis, nitrogen disordering and local magnetic moment

Yu Tao(陶雨) and Li Lei(雷力)†

Institute of Atomic and Molecular Physics, Sichuan University, Chengdu 610065, *China*

(Received 28 February 2025; revised manuscript received 1 April 2025; accepted manuscript online 8 April 2025)

Iron nitride (Fe_xN_y) is a promising candidate for the next generation of ferromagnetic materials. However, synthesizing high-quality bulk iron nitride with tuned structure and magnetic properties remains a challenge. Currently, experimental and theoretical results regarding the magnetic property of iron nitrides remain controversial. With the recent advancements in high-pressure technology, new synthetic pathways to iron nitrides have been proposed. High-pressure synthesis technology provides multidimensional possibilities for tuning the structure and magnetic properties of iron nitrides. This review summarizes recent progress in high-pressure synthesis of iron nitrides, especially the high-pressure solid-state metathesis reaction synthesis (HSM). We have summarized the reaction characteristics of HSM. The HSM reaction exhibits vector synthesis characteristics and promotes nitrogen disorder diffusion at high temperature. Due to this, the HSM reaction can achieve the synthesis of multinary iron-based metal nitrides and regulate the local magnetic moments. It serves as a powerful means for tuning the structure and magnetic properties of iron nitrides. Taking advantage of neutron diffraction in characterizing local magnetic moment and nitrogen disorder in iron nitrides, the relationship between iron local magnetic moment and nitrogen content has been elucidated. Moreover, the development of high-pressure *in-situ* imaging technology based on large-volume press allows the real-time observation of HSM reaction process. In this review, we also report our latest experiments on neutron diffraction and high-pressure *in-situ* image for the study of iron nitrides.

Keywords: iron nitride, high-pressure synthesis

PACS: 83.85.Hf, 82.40.Fp, 77.84.Bw, 75.20.Hr

DOI: 10.1088/1674-1056/adca1c **CSTR:** 32038.14.CPB.adca1c

1. Introduction

Iron is one of the most important metallic elements in the periodic table. As a transition metal, its complex outer electron structure, when bonding with non-metallic elements to form non-metallic compounds, typically exhibits diverse and intricate physical properties.[1,2] Among them, iron's non-metallic compounds are represented by iron oxides, iron carbides, and iron nitrides. Due to the low reactivity of nitrogen under ambient pressure, synthesizing high-quality iron nitride samples with different magnetic properties is challenging. At ambient condition, hydrothermal synthesis, ammonization and chemical vapor deposition are the primary methods for synthesizing iron nitrides. However, it is challenging to obtain high-quality iron nitride samples using ammonization and hydrothermal methods, as the synthesized samples are prone to phase separation and nitrogen deficiency.[3–5] Chemical vapor deposition is typically used to synthesize thin-film iron nitride samples, and the process is relatively complex.[6] Consequently, research on the physical properties of iron nitrides is significantly more limited compared to other non-metallic compounds of iron.

The unique magnetic properties of iron nitrides are the key reasons for their significant attention. They are currently considered promising candidates for next-generation magnetic materials.[7,8] Investigating the specific mechanisms by which nitrogen content regulates the magnetism of iron nitrides is regarded as a fundamental physical problem. Theoretical calculations have been conducted to investigate the magnetic properties of iron nitrides. However, transition metal compounds often cannot have their properties accurately predicted by theoretical calculations, due to their complex outer electron configurations. Theoretical calculations do not match well with experimental results. Specifically, theoretical predictions suggest that α''-$Fe_{16}N_2$ possesses an exceptionally large magnetic moment ($> 3\ \mu_B$), surpassing the Slater–Pauling limit of Fe–Co alloys (2.45 μ_B).[9,10] However, the pure phase of α''-$Fe_{16}N_2$ has not been synthesized experimentally. Giant magnetic moment phenomena have not been observed in most synthesized mixed-phase α''-$Fe_{16}N_2$ nanoparticles or thin-film samples.[11–15] On the other hand, in ε-Fe_3N and γ'-Fe_4N, the synthesis of corresponding ternary iron-based metal nitrides, ε-$Fe_{3-x}M_xN$ and γ'-Fe_3MN (M represents other metal elements), through elemental substitution, is an important approach for tuning the magnetic properties of iron nitrides.[16,17] The substitutional elements do not always couple with Fe atoms in an antiferromagnetic configuration, which would be energetically favored.[18–23] The

†Corresponding author. E-mail: lei@scu.edu.cn

© 2025 Chinese Physical Society and IOP Publishing Ltd. All rights, including for text and data mining, AI training, and similar technologies, are reserved.

role of substitutional elements in tuning the magnetic properties of iron nitrides still requires further investigation. However, at ambient pressure, the synthesis of ternary iron-based metal nitrides is challenging, particularly the synthesis of ε-$Fe_{3-x}M_xN$. Hence, the synthesis of high-quality iron nitrides is crucial to addressing the issues we mentioned above.

In the last decades, advancements in high-pressure technology have provided a new pathway for synthesizing iron nitrides. High-pressure synthesis techniques can effectively overcome the limitations of conventional synthesis methods, as pressure is an important thermodynamic parameter for tuning material properties. The activity of outer-shell electrons changes under high pressure, leading to significant alterations in the interaction rules between atoms. Experimental results indicate Fe tends to bond with N rather than with O under high pressure. Moreover, high-pressure synthesis techniques exhibit unique reaction characteristics not achievable under ambient pressure, offering the potential to tune the properties of iron nitrides from multiple dimensions. Under high-temperature and high-pressure conditions, the nitrogen disordering is significantly enhanced. This disordered diffusion leads to iron nitrides often exhibiting non-stoichiometric compositions. ε-$Fe_3N_{1\pm x}$ is the most typical example. The diffusion of nitrogen causes the nitrogen coordination number around Fe atoms to deviate from the ideal value of 2 in the lattice. Based on the occupancy (occ.) of nitrogen at different Wyckoff positions, the nitrogen coordination number around iron atoms follows a statistical distribution between 0 and 6. The magnetic moment of Fe atoms varies for different coordination numbers. The application of pressure offers a potential route for fine-tuning the magnetic properties of iron nitrides. On the other hand, high-pressure synthesis techniques also exhibit some unique characteristics. High-pressure synthesis techniques exhibit vectorial synthesis characteristics, providing a new pathway for the synthesis of ternary iron-based metal nitrides. In this review, our primary goal is to discuss the advantages of high-pressure synthesis techniques in the fabrication of iron nitrides.

The development of large-scale scientific facilities has also brought new opportunities for the study of iron nitrides. Neutron diffraction offers unique advantages in elucidating the magnetic properties and structure of iron nitrides. This review discusses recent progress we have made in the study of iron nitrides using neutron diffraction. Typically, magnetic data obtained from vibrating sample magnetometer (VSM) or superconducting quantum interference device (SQUID) measurements can only characterize the macroscopic magnetic properties, which cannot directly reflect the magnetic structure of the iron nitrides. Through neutron diffraction, we can obtain information on the local magnetic moments of iron nitrides. In addition, the Shanghai Synchrotron Radiation Facility established the country's first high-temperature and high-pressure large-volume press experimental station. The development of high-pressure *in-situ* imaging technique enables the real-time observation of the HSM reaction process. This provides strong support for a deeper understanding of the role of high pressure in the synthesis of iron nitrides. We briefly discuss the progress made using these techniques in the study of iron nitrides.

This review is organized into the following sections. In Section 2, we introduce two high-pressure synthesis techniques, discussing the advantages of the HSM reaction based on large-volume presses in synthesizing iron nitrides. The application of high-temperature and high-pressure *in-situ* imaging technique in studying the HSM reaction is presented. In Section 3, we discuss the iron nitride structures discovered in current experiments and summarize the synthesis pathways of iron nitrides with different structures. In Section 4, we present the high-pressure synthesis phase diagram of iron nitrides. Unique characteristics of high-pressure methods in the synthesis of iron nitrides are summarized. In Section 5, we examine the magnetic properties of different iron nitrides and compare the magnetism of samples synthesized under ambient pressure and high-pressure conditions. In Section 6, we provide an outlook. Rare-earth-free permanent magnets represent the future direction for the development of permanent magnetic materials, and iron nitride is currently one of the most promising candidates. The synthesis of rare-earth-free permanent magnets using high-pressure synthesis techniques holds great potential for future applications.

2. High-pressure synthesis method

2.1. High-pressure solid-state metathesis reaction based on large-volume presses

A high-pressure solid-state metathesis (HSM) route with novel reaction precursors was first reported in 2009 by Lei and He on the synthesis of GaN.[24] The mechanism and understanding of the HSM reaction have become increasingly refined in the last decade.[25–27] The HSM reaction can be used to synthesize high-quality bulk metal nitrides in large-volume presses. The HSM reaction is represented as follows:[28]

$$AMO + BN \xrightarrow{\text{HPHT}} ABO + MN, \tag{1}$$

$$MO + BN \xrightarrow{\text{HPHT}} BO + MN, \tag{2}$$

where AMO and MO represent ternary and binary metal oxides, respectively, containing M metal cations, BN represents boron nitride, ABO represents ternary metal borates, and MN represents binary metal nitrides. This chemical reaction follows the rules of the double displacement reaction, one of the four major types of chemical reactions. HSM is a unique

chemical reaction that only occurs under high-pressure conditions. The presence of high pressure is a key factor that enables this reaction to occur. Hence, this chemical reaction is a typical demonstration of high pressure's role in tuning material properties. Generally, high pressure reduces the activation energy required for the reaction and helps inhibit the decomposition of the products, since the formation process of iron nitrides is not inherently stable under ambient conditions.

By selecting salts containing different metal cations, the corresponding metal nitrides can be synthesized. A variety of metal nitrides have been synthesized through this reaction, including FeN_x,[29] CoN_x,[30] CrN_x,[31] etc. A typical reaction equation for synthesizing metal nitride is represented as follows:

$$Fe_2O_3 + BN \xrightarrow{\text{HPHT}} \varepsilon\text{-}Fe_3N + B_2O_3 + N_2\uparrow, \quad (3)$$

$$NaCrO_2 + BN \xrightarrow{\text{HPHT}} CrN + NaBO_2 + N_2\uparrow, \quad (4)$$

$$NaCoO_2 + BN \xrightarrow{\text{HPHT}} CoN_x + NaBO_2 + N_2\uparrow. \quad (5)$$

The synthesized product can be easily separated from the byproducts. Figure 1 presents a schematic diagram of the HSM reaction mechanism and an optical image of the product. Product size can reach the millimeter scale using the HSM reaction. The typical sample chamber size is 8 mm, and the synthesized metal nitride can have a maximum diameter of 5 mm. Therefore, iron nitrides synthesized via the HSM reaction can be further characterized by neutron diffraction to determine the magnetic structure, energy dispersive x-ray spectroscopy (EDS) to accurately measure the nitrogen content, synchrotron radiation to assess the bulk modulus, and VSM or SQUID to study magnetic phase transitions.

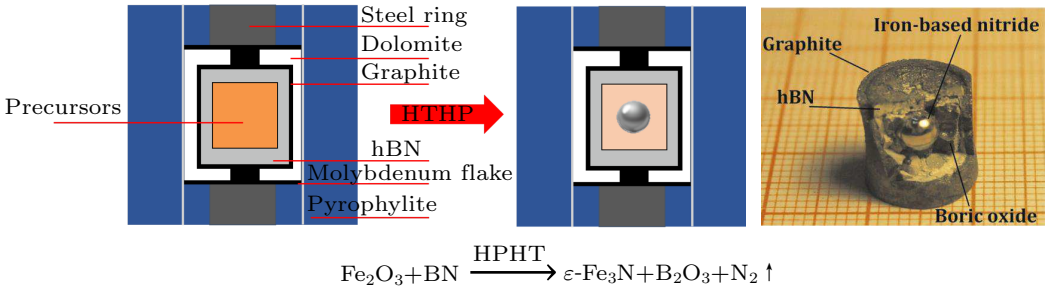


Fig. 1. Schematic diagram of the sample chamber used in the HSM reaction. Optical images of a synthesized iron nitride just recovered from the high-pressure cell in LVP.[34]

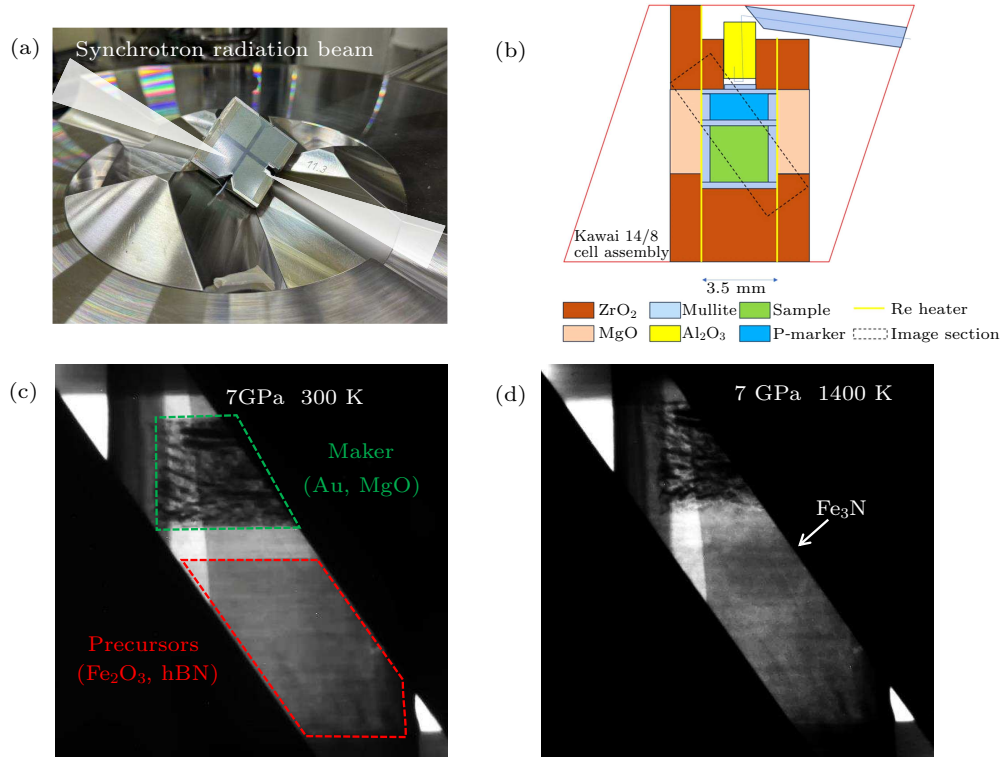


Fig. 2. Panels (a) and (b) illustrate a schematic of the beam path through the cell and the assembly design, while (c) and (d) show *in-situ* imaging of the sample chamber before and after the reaction under 7 GPa conditions, respectively. The red dashed box indicates the reaction precursor, the green dashed box indicates the pressure markers (Au and MgO), and the white dashed box indicates the spherical iron nitride product formed during the reaction.

2.2. High-pressure *in-situ* imaging technique

Due to the enclosed environment of the large-volume press, the formation mechanism of bulk metal nitrides and the HSM reaction mechanism remain not fully understood. Recently, using the high-pressure synchrotron radiation *in-situ* imaging technique based on large volume press at the beamline BL12SW of Shanghai Synchrotron Radiation Facility (SSRF), we successfully observed the entire *in-situ* reaction process of a HSM reaction with the formation of spherical bulk products ($Fe_2O_3 + hBN \xrightarrow{HPHT} \varepsilon\text{-}Fe_3N + B_2O_3 + N_2\uparrow$). The high-pressure *in-situ* imaging technique employs high-energy white beams generated by third-generation synchrotron radiation to penetrate the octahedral pressure medium, enabling real-time observation of the reaction process at high pressures.[35,36] Figure 2(a) illustrates a schematic of the path of the synchrotron radiation beam, while Figs. 2(c) and 2(d) show *in-situ* imaging of the sample chamber before and after the reaction under 7 GPa conditions. The entire formation process of a 1.3 mm diameter metal sphere was observed. Generally, the iron nitride produced by the HSM reaction initially forms as small crystallites that are uniformly distributed within the sample chamber. With the increasing temperature, the iron nitride and other products in the chamber melt. Then, the iron nitride melt coalesces into a large spherical form. By focusing on the key reaction stages, we can optimize the reaction pathway and more effectively control reaction conditions in the future.

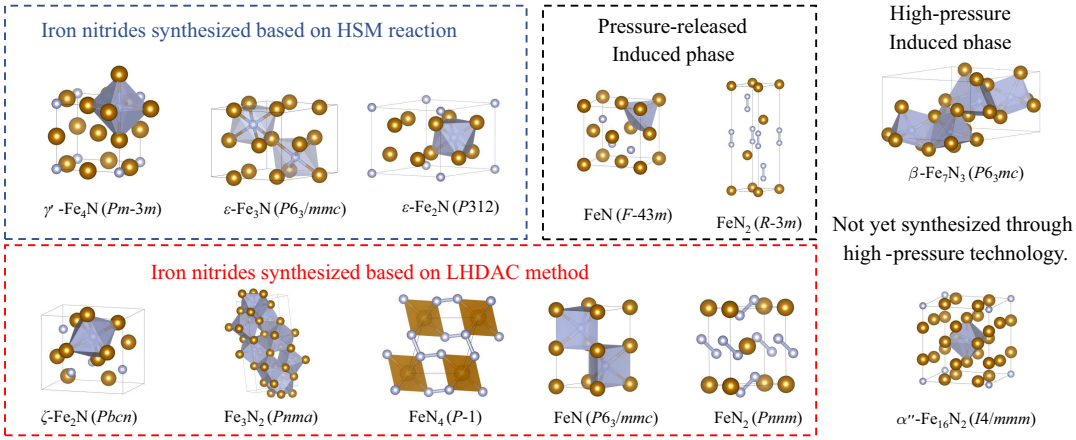


Fig. 3. Experimentally discovered binary iron nitride structures. The blue dashed box represents iron nitride compounds that can be directly synthesized through the HSM reaction,[29,42,43] the red dashed box represents those directly synthesized via LHDAC method,[40,41,44] and the black dashed box represents structures obtained during decompression (which cannot be directly synthesized). β-Fe_7N_3 is derived from ε-Fe_3N and γ'-Fe_4N,[45] while $Fe_{16}N_2$ has not yet been synthesized using high pressure methods.

2.3. Laser heating diamond anvil cell technique

The laser heating diamond anvil cell (LHDAC) technique generates high pressure using a diamond anvil cell (DAC) and directly heats the sample with high-energy laser irradiation. A 1064 nm wavelength YAG laser or a CO_2 laser is generally used. The pressure and temperature achieved by the LHDAC technique are significantly higher than those of large-volume presses. The LHDAC technique currently covers pressure and temperature ranges of 0–300 GPa and 0–4000 K.[37–39] The highest pressure and temperature used for synthesizing iron nitrides are approximately 140 GPa and above 2200 K.[40]

The main purpose of using LHDAC to synthesize iron nitrides is to search for high-energy-density materials that are stable at relatively lower pressures compared to polynitrogen. Due to this, the precursors used in the synthesis of iron nitrides via the LHDAC technique differ from those employed in other methods as well as HSM ratios. It typically uses Fe foil and molecular nitrogen as precursors,[40,41]

$$Fe + N_2 \xrightarrow{HPHT} Fe_xN_y. \tag{6}$$

LHDAC enables the observation of some metastable iron nitride structures under high pressure. During the laser heating process, there is typically a significant temperature gradient within the sample chamber, and the heating temperature cannot be precisely controlled. As a result, iron nitride synthesized using the LHDAC technique is generally in an incomplete, mixed-phase state. Additionally, the sample chamber of the DAC is only a few tens of micrometers in size, which severely limits the available characterization techniques. Generally, only structural information can be obtained through synchrotron radiation. Most of the structures obtained using the LHDAC technique are high-pressure phases and cannot remain stable at ambient pressure. This prevents us from studying the magnetic structures and magnetic phase transitions of these iron nitrides at ambient pressure.

3. Iron nitrides synthesized by high-pressure method

3.1. The ε-$Fe_3N_{1\pm x}$

The ε-$Fe_3N_{1\pm x}$ is one of the most common structures of iron nitride, which remains stable at ambient condition. In the ideal structure of ε-Fe_3N, Fe atoms adopt a hexagonal

close-packed (hcp) arrangement, with nitrogen atoms occupying one-third of the voids within the Fe_6 octahedra in an ordered manner. Each iron atom is coordinated by two nearest-neighbor nitrogen atoms. For this structure, it typically exhibits a non-stoichiometric composition. The nitrogen content can vary within a certain range. ε-Fe_3N, ε-Fe_2N, and ε-Fe_7N_3 represent three common nitrogen contents. They all belong to the ε-$Fe_3N_{1\pm x}$ phase. In this structure, nitrogen atoms exhibit nitrogen diffusion. Taking the $P6_322$ space group as an example, nitrogen atoms can also occupy the 2*b* and 2*d* positions. In the past, both the $P312$ and $P6_322$ space groups were used to describe the structure of ε-$Fe_3N_{1\pm x}$.[46] Powder neutron diffraction experiments have suggested that the $P6_322$ space group provides a better description of the ε-Fe_3N structure.[33] ε-Fe_2N adopts a $P312$ space group structure.[47,48]

The ε-$Fe_3N_{1\pm x}$ is the most common product obtained from the HSM reaction of iron nitride. In 2014, Yin *et al.* reported the preparation of ε-Fe_3N at the millimeter scale through the HSM method. The reaction equation is as follows:[34]

$$NaFeO_2 + BN \xrightarrow{\text{HPHT}} \varepsilon\text{-}Fe_3N + NaBO_2 + N_2\uparrow. \quad (7)$$

Subsequently, it was found that ε-Fe_3N can also be synthesized using Fe_2O_3 or FeOOH as precursors. The reaction equation is as follows:[32,33]

$$Fe_2O_3 + BN \xrightarrow{\text{HPHT}} \varepsilon\text{-}Fe_3N + B_2O_3 + N_2\uparrow, \quad (8)$$

$$FeOOH + BN \xrightarrow{\text{HPHT}} \varepsilon\text{-}Fe_3N + B_2O_3 + H_2\uparrow + N_2\uparrow. \quad (9)$$

In recent years, there has also been a report of high-pressure synthesis of other stoichiometries of ε-$Fe_3N_{1\pm x}$. In 2021, Ma *et al.* reported the synthesis of ε-Fe_2N through an HSM reaction under high pressure and high temperature. The reaction equation is as follows:[42]

$$FeCl_2 + Ca_3N_2 \xrightarrow{\text{HPHT}} \varepsilon\text{-}Fe_2N + CaCl_2 + N_2\uparrow. \quad (10)$$

The synthesis of ε-$Fe_3N_{1\pm x}$ reflects the unique advantages of high pressure in tuning the behavior of nitrogen.

3.2. The γ'-Fe_4N

The γ'-Fe_4N adopts an antiperovskite-like structure with the space group $Pm3m$. In this structure, Fe occupies two distinct sites: 3*d* and 1*b*. Due to the anti-perovskite structure of γ'-Fe_4N, substituting Fe atoms with transition metal elements forming γ'-Fe_3MN can enable the tuning of the properties of γ'-Fe_4N. Hence, γ'-Fe_4N is an ideal candidate for investigating and modulating the magnetic properties of iron nitrides.

A pure phase of γ'-Fe_4N has not yet been synthesized by the high pressure method. On the other hand, Wu *et al.* reported that by introducing nickel oxide into the precursor of the HSM reaction, γ'-Fe_xNi_yN could be obtained in the final product. The reaction equation is as follows:[43]

$$Fe_2O_3 + NiO + BN \xrightarrow{\text{HPHT}} \gamma'\text{-}Fe_3NiN + B_2O_3 + N_2\uparrow. \quad (11)$$

Under the typical temperature and pressure conditions of the HSM reaction for synthesizing iron nitrides, the higher enthalpy of formation of the γ' phase is the possible reason why a single γ' phase has not been successfully synthesized. However, it is feasible to synthesize the pure phase of γ'-Fe_4N through the HSM reaction by tuning the reaction parameters.

3.3. The ζ-Fe_2N

The ζ-Fe_2N adopts a $Pbcn$ space group structure, which are stable under ambient conditions. ζ-Fe_2N and ε-Fe_2N have the same stoichiometry and exhibit similar structures. In both phases, the Fe atoms form a hexagonal close-packed (hcp) structure. The iron (Fe) atom, along with the six adjacent nitrogen (N) atoms, forms an octahedral unit with FeN_6 as the unit. In ζ-Fe_2N, the FeN_6 units share both edges and vertices, while in ε-Fe_2N, the FeN_6 units only share the vertices of the octahedra.[48]

Currently, there are few reports on the high-pressure synthesis of ζ-Fe_2N. According to the report by Laniel *et al.*, ζ-Fe_2N was observed after heating Fe foil and molecular nitrogen using the LHDAC technique at pressures below 17 GPa.[49] At higher pressures, only FeN was detected. Under similar pressure conditions, there have been no reports of ζ-Fe_2N synthesis using large-volume press techniques. According to the report by Schwarz *et al.*, ζ-Fe_2N synthesized at ambient pressure will transform into ε-Fe_2N under high temperature and high pressure.[48] ζ-Fe_2N may not be a stable phase under high pressure.

3.4. The FeN

Theoretically, three possible FeN structures have been predicted: ZnS, NiAs, and NaCl types.[50,51] Among these, the NaCl-type structure is considered the most stable. However, only the NaCl-type FeN structure has not been experimentally observed. In all the reports on the synthesis of iron nitrides using Fe foil and molecular nitrogen as precursors, employing the LHDAC technique, the presence of FeN has been observed. The NiAs-type FeN adopts a $P6_3/mmc$ space group and the ZnS-type FeN adopts an F-43m space group. The crystal structure of NiAs-type FeN shows a trigonal-prismatic coordination of the nitride, while the ZnS-type FeN exhibits a tetrahedral coordination of the nitrogen atoms. The LHDAC technique can only synthesize NiAs-type FeN. The NiAs-type FeN transitions into ZnS-type FeN at ambient conditions.[49] The synthesis of FeN requires a pressure exceeding 30 GPa. This structure remains stable over a wide pressure range. Bykov *et al.* synthesized iron nitrides under pressures up to 130 GPa, where NiAs-type FeN was still observed.[52] Iron nitrides with high nitrogen content are generally considered unstable. Although Laniel *et al.* reported that the ZnS-type FeN structure can exist at ambient pressure, the sample size synthesized using a diamond anvil cell (DAC) is extremely small.

The properties of ZnS-type FeN need to be further characterized in the future.

3.5. The FeN_2 and FeN_4

The N/Fe stoichiometric ratio in FeN_2 and FeN_4 exceeds 1. They exhibit significant structural and property differences compared to other iron nitride compounds. In other iron nitrides, nitrogen primarily exists in the form of interstitial nitrogen atoms, with no interactions between nitrogen atoms. FeN_2 and FeN_4 belong to the class of pernitides. Nitrogen atoms can form N–N bonds. By using the Raman scattering technique, N–N stretching vibrational modes can be detected in iron pernitides.

The primary goal of synthesizing pernitrides is to discover a high-energy-density material that remains stable under ambient pressure.[53,54] The existence of corresponding pernitrides MN_2 has been experimentally observed for other transition metals, such as Pt, Ir, Pd, Os, Rh, Ru, Co, and Ti.[55–59] In 2018, Laniel *et al.* first discovered the existence of FeN_2.[49] The synthesis of FeN_2 and FeN_4 is similar to FeN. The synthesis of pernitrides requires higher pressure ($>$ 50 GPa) and temperature ($>$ 2000 K) conditions than those of FeN. Even the synthesis of FeN_4 requires pressures exceeding 100 GPa. According to Bykov *et al.*, FeN_4 can be synthesized by heating a mixed phase of FeN_2 and FeN or by heating Fe foil with molecular nitrogen. FeN_4 crystallizes in the P-1 space group. Upon decompression to approximately 20 GPa, this structure ceases to exist. FeN_2 exists in two structural forms with space groups *Pnnm* and R-3m. The *Pnnm* phase is directly obtained through laser heating, while the R-3m phase emerges during the decompression process. Even under laser heating at lower pressures, the R-3m structure of FeN_2 cannot be directly synthesized. This phenomenon is similar to the transition between the two structures of FeN. Pernitrides cannot remain stable at ambient pressure and will transform into the ZnS-type FeN during the decompression process.

3.6. The Fe_3N_2

The Fe_3N_2 has an orthorhombic structure with the *Pnma* space group. Fe_3N_2 was observed during the synthesis of pernitrides. This structure forms quadrilateral face-capped trigonal prisms with NFe_7 as the unit. These triangular bipyramids are interconnected by sharing triangular faces and edges. Until the discovery of this structure, there were no theoretical calculations predicting its existence. Fe_3N_2 is thought to be isostructural with chromium carbide Cr_3C_2. In Bykov *et al.*'s report, this structure appeared only in a single experiment, and after subsequent laser heating, the signal from this structure disappeared.[52] The existence of this phase requires further experimental confirmation.

3.7. The β-Fe_7N_3

The β-Fe_7N_3 is synthesized at approximately 41 GPa and 1000 K by laser heating a small amount of Fe-containing ε-Fe_7N_3 or γ'-Fe_4N. The synthesis of β-Fe_7N_3 did not employ Fe foil and molecular nitrogen as precursors.[45] Hence, the structure does not originate from a high-pressure chemical reaction, but rather from a structural phase transition of ε-Fe_7N_3 under high temperature and high pressure.

This structure was characterized using high-pressure *in situ* synchrotron radiation. Multiple new diffraction peaks appeared after laser heating. The structure was compared with that of Fe_7C_3, where the $P6_3mc$, *Pbca* and *Pmcn* space groups were theoretically predicted. This structure matches the $P6_3mc$ space group. At higher pressure, the presence of this phase can still be observed through laser heating. The diffraction peak signals from the β-Fe_7N_3 also became more pronounced. The diffraction peaks of the β-Fe_7N_3 can still be observed up to 140 GPa. When the pressure was reduced to 37 GPa, the signal from this phase almost disappeared. When the pressure was released to ambient pressure, it reverted to ε-Fe_7N_3.

3.8. The α''-$Fe_{16}N_2$ and α'-Fe_8N

The α''-$Fe_{16}N_2$ and α'-Fe_8N crystallize in the $I4/mmm$ space group structure. α''-$Fe_{16}N_2$ is currently the only iron nitride compound that has not been synthesized using high-pressure methods. However, α''-$Fe_{16}N_2$ holds a significant position in the iron-nitrogen compound system. α'-Fe_8N is considered as a highly distorted α-Fe (Im-3m). Approximately 10% of the (0.5, 0.5,0) and (0, 0, 0) sites are randomly occupied by nitrogen atoms. When nitrogen atoms orderly occupy the 2a positions, α'-Fe_8N transforms into α''-$Fe_{16}N_2$. In this structure, Fe occupies three different sites: 4e, 8h, and 4d. Nitrogen atoms form octahedral structures with Fe atoms at the 4e and 8h sites.

The α''-$Fe_{16}N_2$ exhibits an exceptionally high saturation magnetization, even surpassing the limit of Fe–Co alloys described by the Slater–Pauling curve (2.5 μ_B). Neutron diffraction results indicate that the magnetic moment of Fe in α''-$Fe_{16}N_2$ reaches 3.8 μ_B.[60] From an energy perspective, when the nitrogen content in iron nitrides is below 20%, the structure is considered unstable. As a result, no bulk α''-$Fe_{16}N_2$ samples have been synthesized to date. In the synthesized powder or thin-film α''-$Fe_{16}N_2$ samples, a mixed phase of the γ' phase and α-Fe is usually present.[61] Hence, the giant magnetic moment of α''-$Fe_{16}N_2$ remains controversial. High-pressure synthesis methods could be a potential approach for obtaining bulk pure-phase α''-$Fe_{16}N_2$.

4. The general principles of high-pressure synthesis of iron nitride

4.1. The high-pressure synthesis phase diagram of iron nitride

Figure 4 presents the high-pressure synthesis phase diagram of iron nitrides. The dashed lines indicate that there are no distinct boundaries between the synthesized iron nitride structures. The circles and triangles represent synthesis using the LHDAC and LVP techniques, respectively. Overall, the phase diagram can be divided into three synthesis regions. The first region, represented by the orange-red area, corresponds to the synthesis of ε-Fe_3N. ε-Fe_2N and ε-Fe_3N can be regarded as ε-phase iron nitrides synthesized with different nitrogen contents under varying initial conditions. Therefore, high-pressure synthesis techniques could be a potential approach for tuning the nitrogen content in iron nitrides. It is noteworthy that within this temperature and pressure range, ζ-Fe_2N can be synthesized using the LHDAC technique. According to the report by Schwarz *et al.*, the ζ-Fe_2N phase transforms into ε-Fe_2N under high-temperature and high-pressure conditions. Within this temperature and pressure range, thermodynamic or kinetic factors favor the formation of ε-Fe_2N, while the formation of ζ-Fe_2N is suppressed. The second region is the green area, where the synthesized iron nitrides are primarily in the FeN structure. In this region, the presence of Fe_3N_2 and β-Fe_7N_3 has been observed. However, further experimental validation is required to confirm the existence of these two structures. The third region corresponds to the temperature and pressure range above 50 GPa and 2000 K. The iron-nitrogen compounds formed in this region primarily exist in the form of pernitrides. Currently, all known iron pernitrides are unstable under ambient pressure.

The ζ-Fe_2N, ZnS-type FeN, and α''-$Fe_{16}N_2$ have not yet been synthesized using high-pressure methods based on LVP technology. However, these structures can exist under ambient pressure. ζ-Fe_2N and ZnS-type FeN have been successfully synthesized by the high-pressure method, and the LVP technique can cover the corresponding temperature and pressure ranges. On the other hand, although no reports on the high-pressure synthesis of α''-$Fe_{16}N$, its structural similarity to γ-Fe_4N suggests a feasible synthesis pathway. By regulating the denitrification process during γ-Fe_4N formation, it may be possible to obtain α''-$Fe_{16}N_2$. Based on this, we propose three possible methods to achieve the synthesis of these structures.

Melt regulation High-pressure *in-situ* imaging technique indicates that iron nitrides exist as a melt at 5 GPa and 1400 °C. During the transition from the molten state to crystalline iron nitrides, controlling the pressure–temperature (P–T) path can influence the final structure. For example, after forming the melt, maintaining the temperature and reducing the pressure to 2–3 GPa before cooling might induce the formation of ζ-Fe_2N.

Fluid nitrogen encapsulation based on LVP Encapsulating fluid in a large-volume press is not easy. By designing a fluid encapsulation assembly suitable for LVP, liquid nitrogen and Fe powder could be use as precursors, similar to the LHDAC method. This approach might enable the synthesis of ZnS-type FeN.

Denitrification regulation To synthesize α''-$Fe_{16}N_2$, a suitable precursor is required to induce denitrification under high-temperature conditions. Although hBN is the sole nitrogen source in the precursor, its low content would hinder the HSM reaction. Therefore, the denitrification process should occur after the formation of the iron nitride melt. The ideal precursor should possess the following characteristics: it should not interfere with the initial melt formation and should react with nitrogen within the melt to facilitate denitrification, ultimately leading to the formation of α''-$Fe_{16}N_2$.

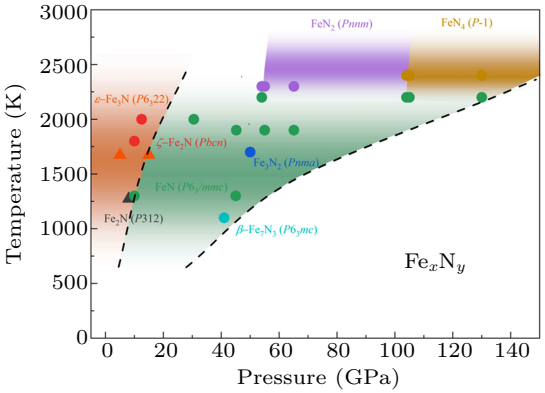


Fig. 4. High-pressure phase diagram for the synthesis of binary iron nitrides. Circles represent the synthesis experiments based on the LHDAC method,[44,45,49,50,52,62,63] while triangles represent synthesis via the HSM reaction.[29,32,42,43] Different colors indicate the primary iron nitride phases synthesized within the corresponding temperature–pressure ranges. The dashed lines represent that the synthesis temperature and pressure boundaries are not precisely defined.

4.2. Diffusion of nitrogen under high pressure

The nitrogen occupation sites and nitrogen content are two key factors influencing the properties of iron nitrides. Under high pressure, high temperatures can promote the disordered diffusion of nitrogen atoms into higher-energy interstitial sites. Neutron diffraction can effectively detect the diffusion behavior of nitrogen atoms. The intensity of the diffraction peaks can be expressed by the following equation:

$$I(hkl) = I_0 \cdot |F_n(hkl)|^2 \cdot L, \tag{12}$$

where $I(hkl)$ denotes the intensity of the corresponding diffraction peak, and F_n represents the structure factor. For x-ray diffraction, F_n is associated with the electron density. Hence, the intensity of the diffraction peaks is proportional to the number of outer-shell electrons of the atoms for x-ray diffraction. Since the number of outer-shell electrons in iron is

much larger than that in nitrogen, the information about nitrogen atoms obtained through x-ray diffraction is very limited. Neutron diffraction involves the interaction of neutrons with atomic nuclei. The structure factor F_n in neutron diffraction is closely related to the neutron scattering cross-section of the atoms as

$$F_n(hkl) = \sum_j b_j \exp(-2\mathrm{i}(hx_j + ky_j + lz_j)). \tag{13}$$

The scattering cross-sections of nitrogen and iron atoms are quite similar (b(Fe) = 11.1 barns, b(N) = 11.5 barns). Through neutron diffraction refinement, detailed information about nitrogen can be obtained. Additionally, because neutrons themselves carry a magnetic moment, they can be used to probe the magnetic structure of the sample. Therefore, neutron diffraction can be used to study the effects of nitrogen diffusion on the magnetic and mechanical properties of iron nitrides.

In recent years, the disordered diffusion of nitrogen in iron nitrides under high temperature and high-pressure conditions has been studied by using neutron powder diffraction techniques (Table 1).[33,43,46,64] For the $P6_322$ space group of ε-Fe_3N, the ideal structure has iron occupying the 6g position and nitrogen occupying the 2c position. Neutron diffraction results indicate that in high-pressure synthesized ε-Fe_3N, nitrogen atoms can diffuse into the 2d and 2b sites. At ambient conditions, occupation of the 2d site is energetically prohibited. However, in iron nitrides synthesized under high pressure, nitrogen atoms can diffuse into the 2d site. The diffusion of nitrogen atoms alters the coordination environment of Fe atoms. The coordination number of N around Fe atoms can vary from 0 to 6, resulting in seven possible configurations. Recently, we synthesized ε-$Fe_3N_{1.422}$ with a higher nitrogen content under higher temperature and pressure conditions. The EDS spectroscopy results indicate a Fe:N stoichiometric ratio of 3:1.430, which is consistent with the neutron diffraction results. Here, we adopt the neutron pattern refinement data as the final reference. We performed refinements of ε-$Fe_3N_{1.422}$ considering both the $P312$ and $P6_322$ space group structures. The $P6_322$ structure exhibits a lower χ^2. Neutron diffraction refinement results indicate that higher pressure and temperature significantly promote nitrogen diffusion behavior. The nitrogen content at the 2d site is significantly increased. Figure 5(d) presents the probability of different nitrogen coordination numbers, derived from statistical analysis based on Rietveld refinement of powder neutron diffraction data.

The disordered diffusion of nitrogen offers two potential approaches for tuning the magnetism of iron nitrides. First, the statistical distribution of nitrogen coordination numbers around Fe atoms changes as a direct result of nitrogen diffusion. Different coordination numbers significantly alter the local environment of Fe atoms, modulating their magnetic moments. Second, nitrogen diffusion may enable nitrogen atoms to occupy Wyckoff sites that are inaccessible under ambient condition, expanding the range of nitrogen content regulation. Taking ε-$Fe_3N_{1\pm x}$ as an example, if more nitrogen atoms diffuse and occupy the 2b and 2d sites, the nitrogen content could potentially exceed the commonly assumed 50% limit. Since nitrogen content is a critical factor influencing the magnetic moments of iron nitrides, this regulation approach offers new possibilities for magnetic property optimization.

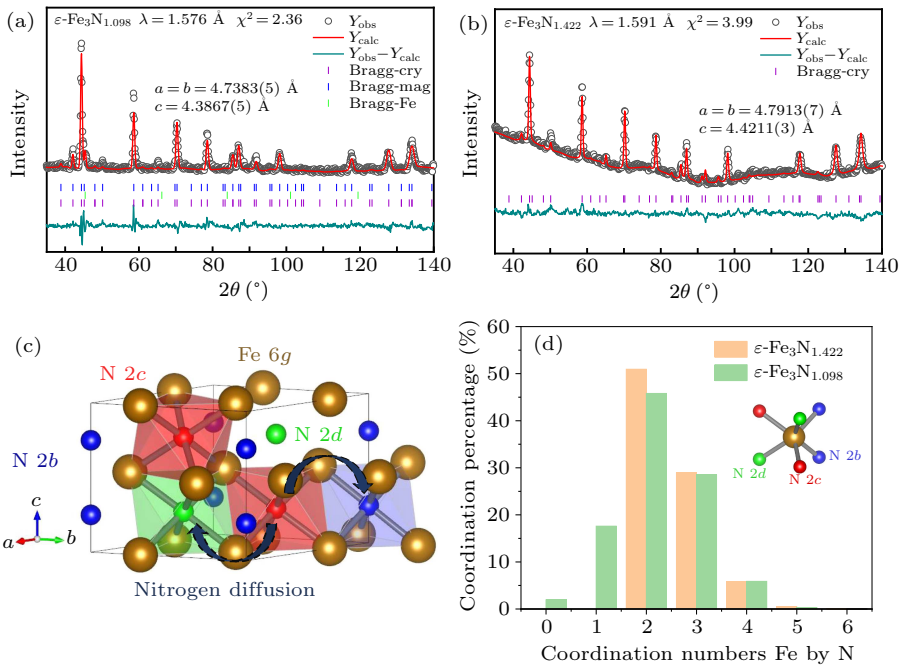


Fig. 5. (a) Neutron powder diffraction refinement pattern of ε-$Fe_3N_{1.098}$.[33] (b) Neutron powder diffraction refinement pattern of ε-$Fe_3N_{1.422}$ [this work]. (c) Atomic occupancy diagram of ideal ε-Fe_3N with $P6_322$ space group structure. (d) Statistical distribution of Fe atoms corresponding to different nitrogen coordination numbers calculated from the refined neutron powder diffraction data. ε-$Fe_3N_{1.098}$ was synthesized under conditions of 15 GPa and 1673 K. ε-$Fe_3N_{1.422}$ was synthesized under conditions of 15 GPa and 1700 K.

Table 1. The atomic site occupancy information for Fe and N based on the refinement of neutron powder diffraction data.[33] The values in parentheses represent the synthesis temperature and pressure conditions for ε-$Fe_3N_{1\pm x}$.

Atom	Wyckoff	x	y	z	occ.
ε-$Fe_3N_{1.098}$ (5 GPa, 1673 K)					
Fe	6*g*	1/3	0	0	1
N	2*c*	1/3	2/3	1/4	0.804(24)
N	2*b*	0	0	1/4	0.264(36)
N	2*d*	2/3	1/3	1/4	0.030(18)
ε-$Fe_3N_{1.422}$ (15 GPa, 1700 K)					
Fe	6*g*	1/3	0	0	0.875(07)
N	2*c*	1/3	2/3	1/4	1
N	2*b*	0	0	1/4	0.175(31)
N	2*d*	2/3	1/3	1/4	0.069(30)

4.3. Substitution of iron under high pressure

Substituting iron atoms with other transition metals is an effective method for tuning the properties of iron nitrides. However, synthesizing ternary iron-based metal nitrides at ambient condition is challenging. Although theoretical calculations have predicted the properties of most ternary iron-based metal nitrides, the number of ternary iron-based metal nitrides synthesized experimentally remains quite limited. Moreover, most of the synthesized compounds adopt the γ'-$Fe_{4-x}M_xN$ structure. The synthesis of ε-$Fe_{3-x}M_xN$ remains even more limited. The vectorial synthesis characteristic of the HSM reaction offers a novel pathway for the synthesis of ternary iron-based metal nitrides. If we regard the single HSM reaction as a "vector", the addition of HSM_1 and HSM_2 obeys the parallelogram law as shown in Fig. 6. Based on the vector rule of the HSM reaction, ternary ε-$Fe_{3-x}Co_xN$, γ'-$Fe_{4-x}Ni_xN$ and ε-$Fe_{3-x}Ni_xN$ have been successfully synthesized.[34,43]

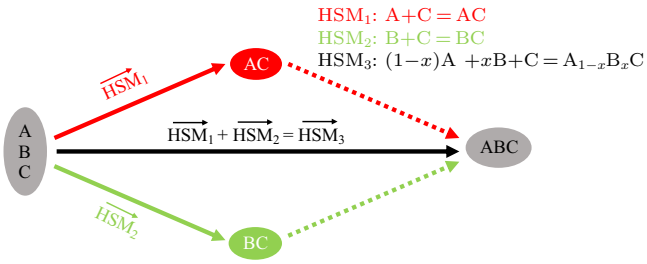


Fig. 6. Schematic diagram of vector synthesis of HSM reactions.

The vectorial synthesis characteristics of the HSM reaction possess certain unique advantages that are not available in other methods. Generally, the formation rules of alloys can be described using the Hume–Rothery rules, where atomic radius is an important factor influencing alloy formation. Metals with significantly different atomic radii cannot form alloys. Since the HSM reaction occurs under high-pressure conditions, pressure can regulate the differences in atomic radii. Hence, the synthesis of iron-based metal nitrides via the HSM reaction can overcome this limitation to some extent. It enables the synthesis of multinary iron-based metal nitrides that cannot be synthesized at ambient pressure. Moreover, the precursors used in the HSM reaction are the corresponding metal oxides, which are readily available. This makes it easier to design new HSM reaction to synthesize multinary metal nitrides. The synthesis of high-entropy nitrides represents a potential future application of the HSM reaction. High-entropy alloys have attracted significant attention in recent years due to their exceptional properties. However, reports on the synthesis of high-entropy nitrides remain scarce.[65–68] Based on the vectorial synthesis characteristics, one can synthesize iron-based high-entropy metal nitrides using the HSM reactions.

5. Magnetic properties of iron nitrides synthesized by high-pressure method

Nitrogen is a crucial factor influencing the magnetic properties of iron nitrides. Among the iron nitrides that are stable at ambient pressure, all exhibit ferromagnetism except for ζ-Fe_2N. The exact mechanism by which nitrogen influences the magnetism of iron nitrides is not yet well understood. Specifically, there are significant discrepancies in the calculated magnetic moments of α''-$Fe_{16}N_2$ based on different theoretical models, and the magnetic phase transition behavior of ζ-Fe_2N remains controversial.[69] Figure 7 presents the experimentally measured magnetic moments of iron nitrides with different structures. The circles represent magnetic moments measured by neutron diffraction, while the triangles represent those measured using VSM techniques. Since single-phase bulk or powder α''-$Fe_{16}N_2$ has not yet been synthesized, the macroscopic magnetic moment measured by VSM does not directly reflect the intrinsic magnetic moment of α''-$Fe_{16}N_2$. Therefore, Fig. 7 does not include the VSM-measured magnetic moment of α''-$Fe_{16}N_2$. The red-outlined points represent samples synthesized under high-pressure conditions, while other solid points represent samples synthesized at ambient pressure. The measured magnetic properties of iron nitride samples synthesized by different methods vary significantly. Overall, if we take the highest measured magnetic moment as a reference, the magnetic moment of iron nitrides tends to decrease as the

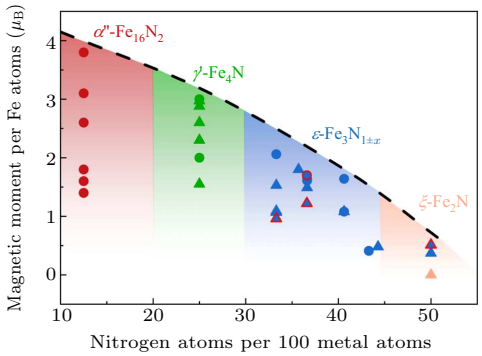


Fig. 7. The relationship between the magnetic moment of iron nitrides and nitrogen content. Circles represent magnetic moments obtained from neutron diffraction,[46,64,70–73] while triangles represent those measured using the VSM method.[74–84] Solid points with red outlines indicate samples synthesized under high-pressure conditions, whereas other solid points represent samples synthesized at ambient pressure.

nitrogen content increases. This trend can also be observed in ε-$Fe_3N_{1\pm x}$. With a variable nitrogen content within a certain range, the magnetic moment of ε-$Fe_3N_{1\pm -x}$ similarly decreases as x increases.

Currently, the synthesized α''-$Fe_{16}N_2$ samples show significant discrepancies in the measured magnetic moment, leading to considerable debate over the existence of its giant magnetic moment. As shown in Fig. 5, the possibility of α''-$Fe_{16}N_2$ exhibiting a giant magnetic moment remains relatively high. It is common for the magnetic moment of iron nitrides synthesized using different methods to vary significantly, particularly when measured by VSM. VSM generally measures the macroscopic magnetic moment, which can be influenced by numerous factors, including sample quality, microstructure, and impurities. This phenomenon is also evident in other iron nitride structures. From an overall perspective, the magnetic moment of iron nitrides tends to decrease with increasing nitrogen content (Table 2). Therefore, the presence of a large magnetic moment in low-nitrogen-content α''-$Fe_{16}N_2$ is plausible. To resolve the ongoing debate, it is essential to synthesize high-quality, pure-phase α''-$Fe_{16}N_2$ samples using high-pressure techniques and further verify their magnetic properties through neutron diffraction.

Table 2. The space group structures, lattice parameters, atomic site occupancy, magnetism, and magnetic moments of typical iron nitrides. The magnetic moment (μ_B) corresponds to the maximum magnetic moment reported experimentally for this structure.

Phase	α''-$Fe_{16}N_2$	γ'-Fe_4N	ε-Fe_3N	ε-Fe_2N	ζ-Fe_2N
Space group	*I*4/*mmm*	*Pm*-3*m*	$P6_322$	*P*312	*Pbcn*
Lattice constant	$a=b=5.72$ Å $c=6.29$ Å[13]	$a=b=c=3.79$ Å[85]	$a=b=4.7383$ Å $c=4.3868$ Å[33]	$a=b=4.77670$ Å $c=4.41790$ Å[42]	$a=4.423$ Å $b=5.531$ Å $c=4.821$ Å[86]
Fractional atomic coordinates	Fe_1(0, 0, 0.2898) Fe_2(0.2449, 0.2449, 0) Fe_3(0, 1/2, 1/4) N(0, 0, 0)[14]	Fe_1(1/2, 0, 0) Fe_2(1/2, 1/2, 1/2) N(0, 0, 0)[85]	Fe(0.31886, 0, 0) N_1(1/3, 2/3, 1/4) N_2(0, 0, 1/4) N_3(2/3, 1/3, 1/4)[33]	Fe(0, 2/3, 1/4) N_1(2/3, 1/3, 0) N_2(1/3, 2/3, 1/2) N_3(0, 0, 0)[42]	Fe(0.24, 0.128, 0.0827) N(0, 0.364, 0.25)[86]
Magnetic ordering	FM	FM	FM	FM	PM
Moment (μ_B)	3.8[14]	2.97[80]	1.7[33]	0.51[42]	0[84]

6. Summary and outlook

In this review, we have summarized the recent progress made in the high-pressure synthesis, structure and magnetic properties of iron nitrides, including the application of high-pressure and high-temperature *in-situ* imaging technique based on large-volume presses. The high-pressure synthesis phase diagram of iron nitrides has been presented, and the synthetic conditions for different structures of iron nitride have been summarized. Combined with our recent experiments in the neutron diffraction of iron nitrides, this review highlights that high-pressure synthesis can promote the disordering diffusion of nitrogen at high temperature. Controlling nitrogen diffusion under high pressure may serve as a potential approach for tuning the structure and magnetic properties of iron nitrides. Additionally, the vectorial reaction characteristics of HSM synthesis offer unique advantages in the formation of high-entropy iron-based metal nitrides. Iron nitride is currently one of the most promising candidates for high-performance rare-earth-free magnetic materials. The high-pressure synthesis method could be the key technique for achieving bulk magnetic-tunable iron-based nitride materials.

Acknowledgements

We thank Prof. Leiming Fang for his help in the neuron diffraction experiments. We thank Dr. Chunyin Zhou for his help in high-pressure *in-situ* imaging experiments. We thank Prof. Duanwei He for his help in LVP experiments. This work was financially supported by the National Natural Science Foundation of China (Grant Nos. 12374013 and U2030107) and the Fundamental Research Funds for the Central University (Grant No. 2020SCUNL107). The high-pressure *in-situ* imaging experiments were conducted at BL12SW of SSRF (Proposal No. 2024-SSRF-PT-505499). The NPD experiments were supported by Chinese Academy of Engineering Physics.

References

[1] Takagi R, Hirakida R, Settai Y, Oiwa R, Takagi H, Kitaori A, Yamauchi K, Inoue H, Yamaura J, Nishio-Hamane D, Itoh S, Aji S, Saito H, Nakajima T, Nomoto T, Arita R and Seki S 2025 *Nat. Mater.* **24** 63
[2] Koemets E, Leonov I, Bykov M, Bykova E, Chariton S, Aprilis G, Fedotenko T, Clément S, Rouquette J, Haines J, Cerantola V, Glazyrin K, McCammon C, Prakapenka V B, Hanfland M, Liermann H P, Svitlyk V, Torchio R, Rosa A D, Irifune T, Ponomareva A V, Abrikosov I A, Dubrovinskaia N and Dubrovinsky L 2021 *Phys. Rev. Lett.* **126** 106001
[3] Zieschang A M, Bocarsly J D, Dürrschnabel M, Molina-Luna L, Kleebe H J, Seshadri R and Albert B 2017 *Chem. Mater.* **29** 621
[4] Mukasyan A S, Roslyakov S, Pauls J M, Gallington L C, Orlova T, Liu X, Dobrowolska M, Furdyna J K and Manukyan K V 2019 *Inorg. Chem.* **58** 5583
[5] Chambers M S, Hunter R D, Hollamby M J, Pauw B R, Smith A J, Snow T, Danks A E and Schnepp Z 2022 *Inorg. Chem.* **61** 6742
[6] Nadzri N I M, Ibrahim D M S and Sompon S 2019 *OP Conf. Ser.: Mater. Sci. Eng.* **701** 012047
[7] Wojciechowski P and Lewandowski M 2022 *Crystal Growth & Design* **22** 4618
[8] Bhattacharyya S 2015 *J. Phys. Chem. C* **119** 1601
[9] Sims H, Butler W H, Richter M, Koepernik K, Şaşıoğlu E, Friedrich C and Blügel S 2012 *Phys. Rev. B* **86** 174422
[10] Sakuma A 1996 *J. Appl. Phys.* **79** 5570
[11] Ji N, Allard L F, Lara-Curzio E and Wang J P 2011 *Appl. Phys. Lett.* **98** 092506
[12] Coey J M D 1994 *J. Appl. Phys.* **76** 6632
[13] Hang X, Matsuda M, Held J T, Mkhoyan K A and Wang J P 2020 *Phys. Rev. B* **102** 104402

[14] Hiraka H, Ohoyama K, Ogata Y, Ogawa T, Gallage R, Kobayashi N, Takahashi M, Gillon B, Gukasov A and Yamada K 2014 *Phys. Rev. B* **90** 134427
[15] Ogawa T, Ogata Y, Gallage R, Kobayashi N, Hayashi N, Kusano Y, Yamamoto S, Kohara K, Doi M, Takano M and Takahashi M 2013 *Appl. Phys. Express* **6** 073007
[16] Zhang C S, Yan M F, You Y, Chen H T, Zhang F Y, Bai B, Chen L, Long Z and Li R W 2014 *J. Alloys Compd.* **615** 854
[17] Dos Santos A V and Kuhnen C A 2009 *Journal of Solid State Chemistry* **182** 3183
[18] Gajbhiye N S, Ningthoujam R S and Bhattacharyya S 2006 *Hyperfine Interact.* **164** 17
[19] Guo K, Rau D, Toffoletti L, Müller C, Burkhardt U, Schnelle W, Niewa R and Schwarz U 2012 *Chem. Mater.* **24** 4600
[20] Houben A, Burghaus J and Dronskowski R 2009 *Chem. Mater.* **21** 4332
[21] Houben A, Müller P, Von Appen J, Lueken H, Niewa R and Dronskowski R 2005 *Angew Chem. Int. Ed.* **44** 7212
[22] Lei X, Pan X, Ye Z, Yang X, Chen X, Shi Z and Yang H 2019 *ChemistrySelect* **4** 5945
[23] Schwarz U, Guo K, Clark W P, Burkhardt U, Bobnar M, Castillo R, Akselrud L and Niewa R 2019 *Materials* **12** 1993
[24] Lei L and He D 2009 *Crystal Growth & Design* **9** 1264
[25] Zhang L, Cheng Y, Lei L, Wang X, Hu Q, Wang Q, Ohfuji H, Kojima Y, Zhang Q, Zeng Z, Peng F, Kou Z, He D and Irifune T 2018 *Crystal Growth & Design* **18** 1843
[26] Lei L, Yin W, Jiang X, Lin S and He D 2013 *Inorg. Chem.* **52** 13356
[27] Jia X, Zhang L, Tian Y, Wu B, Tao Y, He D, Yang B, Boi F S and Lei L 2024 *RSC Adv.* **14** 7490
[28] Lei L and Zhang L 2018 *Matter and Radiation at Extremes* **3** 95
[29] Yin W, Lei L, Jiang X, Liu P, Liu F, Li Y, Peng F and He D 2014 *High Pressure Research* **34** 317
[30] Wu B, Zhang F, Hu Q, Tang Q, Liu S, Xiang X, Xia Y, Fang L, Ohfuji H, Irifune T and Lei L 2021 *J. Appl. Phys.* **129** 105901
[31] Wang S, Yu X, Zhang J, Chen M, Zhu J, Wang L, He D, Lin Z, Zhang R, Leinenweber K and Zhao Y 2012 *Phys. Rev. B* **86** 064111
[32] Zhang H, Wu B, Liu J, Liu Z, Boi F S, He D, Irifune T and Lei L 2023 *Inorg. Chem.* **62** 6263
[33] Lei L, Zhang L, Gao S, Hu Q, Fang L, Chen X, Xia Y, Wang X, Ohfuji H, Kojima Y, Redfern S A T, Zeng Z, Chen B, He D and Irifune T 2018 *J. Alloys Compd.* **752** 99
[34] Zhang L, Gao S, Hu Q, Qi L, Feng L and Lei L 2017 *Materials Chemistry and Physics* **197** 94
[35] Yang K, Dong Z H, Zhou C Y, Zhao Z L, Liang D X, Cao S C and Li A G 2024 *Nucl. Sci. Tech.* **35** 98
[36] Tai R Z and Zhao Z T 2024 *Nucl. Sci. Tech.* **35** 137
[37] Lei L, Tang Q Q, Zhang F, Liu S, Wu B B and Zhou C Y 2020 *Chin. Phys. Lett.* **37** 068101
[38] Laniel D, Geneste G, Weck G, Mezouar M and Loubeyre P 2019 *Phys. Rev. Lett.* **122** 066001
[39] Ji C, Adeleke A A, Yang L, Wan B, Gou H, Yao Y, Li B, Meng Y, Smith J S, Prakapenka V B, Liu W, Shen G, Mao W L and Mao H 2020 *Sci. Adv.* **6** eaba9206
[40] Bykov M, Bykova E, Aprilis G, Glazyrin K, Koemets E, Chuvashova I, Kupenko I, McCammon C, Mezouar M, Prakapenka V, Liermann H P, Tasnádi F, Ponomareva A V, Abrikosov I A, Dubrovinskaia N and Dubrovinsky L 2018 *Nat. Commun.* **9** 2756
[41] Laniel D, Dewaele A, Anzellini S and Guignot N 2018 *J. Alloys Compd.* **733** 53
[42] Ma T, Yin Y, Hong F, Zhu P and Yu X 2021 *ACS Omega* **6** 12591
[43] Wu B, Lei L, Zhang F, Tang Q, Liu S, Pu M, He D, Xia Y, Fang L, Ohfuji H and Irifune T 2021 *Matter and Radiation at Extremes* **6** 038401
[44] Laniel D, Dewaele A and Garbarino G 2018 *Inorg. Chem.* **57** 6245
[45] Minobe S, Nakajima Y, Hirose K and Ohishi Y 2015 *Geophysical Research Letters* **42** 5206
[46] Leineweber A, Jacobs H, Hüning F, Lueken H and Kockelmann W 2001 *J. Alloys Compd.* **316** 21
[47] Wang X, Wang Y, Kan X, Qian L, Zhang Z, Zheng G, Feng S, Lv Q, Yang Y and Liu X 2021 *J. Mater Sci: Mater. Electron* **32** 28144
[48] Schwarz U, Wosylus A, Wessel M, Dronskowski R, Hanfland M, Rau D and Niewa R 2009 *Eur. J. Inorg. Chem.* **2009** 1634
[49] Laniel D, Dewaele A, Anzellini S and Guignot N 2018 *J. Alloys Compd.* **733** 53
[50] Kartsev A, Feya O D, Bondarenko N and Kvashnin A G 2019 *Phys. Chem. Chem. Phys.* **21** 5262
[51] Lambrecht W R L, Miao M S and Lukashev P 2005 *J. Appl. Phys.* **97** 10
[52] Bykov M, Bykova E, Aprilis G, Glazyrin K, Koemets E, Chuvashova I, Kupenko I, McCammon C, Mezouar M, Prakapenka V, Liermann H P, Tasnádi F, Ponomareva A V, Abrikosov I A, Dubrovinskaia N and Dubrovinsky L 2018 *Nat. Commun.* **9** 2756
[53] Wessel M and Dronskowski R 2011 *Chemistry A European J.* **17** 2598
[54] Wang Z, Li Y, Li H, Harran I, Jia M, Wang H, Chen Y, Wang H and Wu N 2017 *J. Alloys Compd.* **702** 132
[55] Niwa K, Suzuki K, Muto S, Tatsumi K, Soda K, Kikegawa T and Hasegawa M 2014 *Chemistry A European J.* **20** 13885
[56] Niwa K, Dzivenko D, Suzuki K, Riedel R, Troyan I, Eremets M and Hasegawa M 2014 *Inorg. Chem.* **53** 697
[57] Crowhurst J C, Goncharov A F, Sadigh B, Evans C L, Morrall P G, Ferreira J L and Nelson A J 2006 *Science* **311** 1275
[58] Crowhurst J C, Goncharov A F, Sadigh B, Zaug J M, Aberg D, Meng Y and Prakapenka V B 2008 *J. Mater. Res.* **23** 1
[59] Bhadram V S, Kim D Y and Strobel T A 2016 *Chem. Mater.* **28** 1616
[60] Hang X, Matsuda M, Held J T, Mkhoyan K A and Wang J P 2020 *Phys. Rev. B* **102** 104402
[61] Ji N, Allard L F, Lara-Curzio E and Wang J P 2011 *Appl. Phys. Lett.* **98** 092506
[62] Niwa K, Terabe T, Kato D, Takayama S, Kato M, Soda K and Hasegawa M 2017 *Inorg. Chem.* **56** 6410
[63] Clark W P, Steinberg S, Dronskowski R, McCammon C, Kupenko I, Bykov M, Dubrovinsky L, Akselrud L G, Schwarz U and Niewa R 2017 *Ingew Chem. Int. Ed.* **56** 7302
[64] Leineweber A, Jacobs H, Hüning F, Lueken H, Schilder H and Kockelmann W 1999 *J. Alloys Compd.* **288** 79
[65] George E P, Raabe D and Ritchie R O 2019 *Nat. Rev. Mater.* **4** 515
[66] Wang X, Zhan Z, Cao H and Zhang Y 2024 *Ceramics International* **50** 14948
[67] Moskovskikh D, Vorotilo S, Buinevich V, Sedegov A, Kuskov K, Khort A, Shuck C, Zhukovskyi M and Mukasyan A 2020 *Sci. Rep.* **10** 19874
[68] Zhao L, Yi M, Zhang C, Shan T, Zhang J, Yang D, Wang J, Bai Y, Guo Q and Xu C 2025 *Ceramics International* S0272884225001749
[69] Wang W, Kan X, Liu X, Dao Y, Feng S, Li Y, Liu C, Shezad M, Zhang Z and Mehmood Ur Rehman K 2020 *Appl. Phys. Lett.* **117** 122408
[70] Lei L, Zhang L, Gao S, Hu Q, Fang L, Chen X, Xia Y, Wang X, Ohfuji H, Kojima Y, Redfern S A T, Zeng Z, Chen B, He D and Irifune T 2018 *J. Alloys Compd.* **752** 99
[71] Hiraka H, Ohoyama K, Ogata Y, Ogawa T, Gallage R, Kobayashi N, Takahashi M, Gillon B, Gukasov A and Yamada K 2014 *Phys. Rev. B* **90** 134427
[72] Hang X, Matsuda M, Held J T, Mkhoyan K A and Wang J P 2020 *Phys. Rev. B* **102** 104402
[73] Frazer B C 1958 *Phys. Rev.* **112** 751
[74] Zieschang A M, Bocarsly J D, Dürrschnabel M, Molina-Luna L, Kleebe H J, Seshadri R and Albert B 2017 *Chem. Mater.* **29** 621
[75] Yamaguchi K, Yui T, Yamaki K, Kakeya I, Kadowaki K and Suemasu T 2007 *Journal of Crystal Growth* **301–302** 597
[76] Wang W, Kan X, Liu X, Dao Y, Feng S, Li Y, Liu C, Shezad M, Zhang Z and Mehmood Ur Rehman K 2020 *Appl. Phys. Lett.* **117** 122408
[77] Lei X, Ye Z, Qie Y, Fan Z, Chen X, Shi Z and Yang H 2019 *J. Mater Sci: Mater Electron* **30** 277
[78] Kurian S and Gajbhiye N S 2010 *Chem. Phys. Lett.* **493** 299
[79] Kumaresan L, Shanmugavelayutham G and Saravanan P 2022 *Appl. Phys. A* **128** 1073
[80] Jiang Y and Jiang L 2019 *AIP Advances* **9** 035215
[81] Jiang Y and Jiang L 2019 *IEEE Trans. Magn.* **55** 4003907
[82] Dirba I, Yazdi M B, Radetinac A, Komissinskiy P, Flege S, Gutfleisch O and Alff L 2015 *J. Magn. Magn. Mater.* **379** 151
[83] Dirba I, Chandra C K, Ablets Y, Kohout J, Kmječ T, Kaman O and Gutfleisch O 2023 *J. Phys. D: Appl. Phys.* **56** 025001
[84] Naganuma H, Endo Y, Nakatani R, Kawamura Y and Yamamoto M 2004 *Science and Technology of Advanced Materials* **5** 83
[85] Jacobs H, Rechenbach D and Zachwieja U 1995 *J. Alloys Compd.* **227** 10
[86] Hasegawa M and Yagi T 2005 *J. Alloys Compd.* **403** 131